NANO LETTERS

LETTER

pubs.acs.org/NanoLett

Graphene Bimetallic-like Cantilevers: Probing Graphene/Substrate Interactions

Hiram Conley,[†] Nickolay V. Lavrik,[‡] Dhiraj Prasai,[†] and Kirill I. Bolotin[†,*]

[†]Department of Physics and Astronomy, Vanderbilt University, Nashville, Tennessee 37235, United States

[‡]Center for Nanophase Materials Sciences, Oak Ridge National Laboratory, Oak Ridge, Tennessee 37830, United States

Supporting Information

ABSTRACT: The remarkable mechanical properties of graphene, the thinnest, lightest, and strongest material in existence, are desirable in applications ranging from composite materials to sensors and actuators. Here, we demonstrate that these mechanical properties are strongly affected by the interaction with the substrate onto which graphene is deposited. By measuring the temperature-dependent deflection of graphene/substrate "bimetallic" cantilevers we determine strain, thermal expansion coefficient, and the adhesion force acting on graphene films attached to a substrate. Graphene deposited on silicon nitride (SiN_x) is under much larger strain, $\varepsilon_g \sim 1.5 \times 10^{-2}$, compared to graphene on gold (Au), $\varepsilon_g < 10^{-3}$. The thermal expansion coefficient α_g of graphene attached to SiN_x is found to be negative, in the range from $(-5 \ldots -1) \times 10^{-6} K^{-1}$ and smaller in magnitude than α_g of suspended graphene. We also estimate the interfacial shear strength of the graphene/SiN_x interface to be ~1 GPa at room temperature.

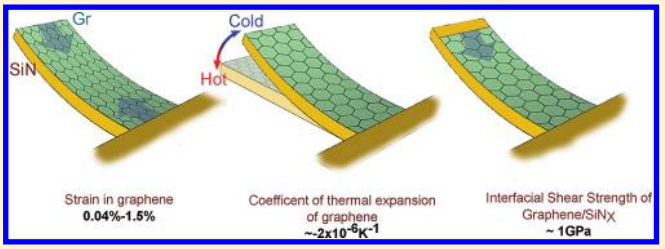

KEYWORDS: Graphene, bimetallic, cantilevers, strain, thermal expansion, interfacial shear strength

Graphene, a two-dimensional carbon allotrope, features a remarkable combination of mechanical properties: it is the thinnest[1] and the strongest[2] material ever measured. It has been suggested that these properties may find applications ranging from light yet strong composite materials[3,4] to nanoelectromechanical actuators and sensors.[2,5,6] However, while most of the proposed applications require an understanding and control of the mechanical properties of graphene films deposited on substrates, the majority of experiments probe suspended graphene films, either by pushing them with the tip of an atomic force microscope[2] or by measuring their mechanical resonant frequency.[5−7] At the same time, since every atom in graphene belongs to the surface and is affected by its local environment, the presence of the substrate can significantly alter the mechanical properties of graphene, perturb the phonon spectrum, and thus affect the thermal expansion coefficient of graphene, or change graphene's Young's modulus.[8] The mechanical interaction with the substrate can even affect the electronic properties of graphene. It has been demonstrated that large localized strains in graphene produce a pseudomagnetic field.[9,10] However, despite the initial progress the mechanics of the graphene/substrate interaction remains largely unexplored because of the lack of adequate experimental techniques.

Here, we develop a technique to probe the mechanical properties of graphene films attached to substrates. At the heart of this technique are suspended bimetallic-like cantilevers consisting of a well-characterized substrate layer and a layer of test material, such as graphene. By measuring the deflection of these cantilevers as a function of temperature we are able to extract graphene's in-plane isotropic strain, coefficient of thermal expansion, and estimate the frictional forces between graphene and the substrate.

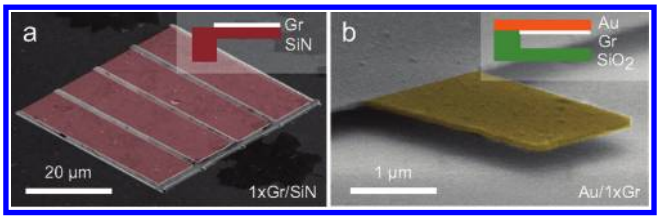

Figure 1. SEM images of the graphene bimetallic-like cantilevers following fabrication. (a) Single layer graphene/silicon nitride ($1\times$Gr/SiN_x) cantilever, the suspended part false-colored red. (b) Gold/Single layer graphene (Au/$1\times$Gr) cantilever, the suspended part false-colored yellow. Insets: Cartoon views of the devices.

To explore the interaction of graphene with a range of substrates, we studied cantilevers with either a silicon nitride (SiN_x) or gold (Au) substrates and either single ($1\times$Gr), double ($2\times$Gr), or triple ($3\times$Gr) layer graphene films attached to the substrate. We fabricated and measured four $1\times$Gr/SiN_x devices, one $2\times$Gr/SiN_x device, two $3\times$Gr/SiN_x devices, and nine $1\times$Gr/Au devices (Figure 1a,b).

Received: July 26, 2011
Revised: September 30, 2011

dx.doi.org/10.1021/nl202562u | *Nano Lett.* XXXX, XXX, 000–000

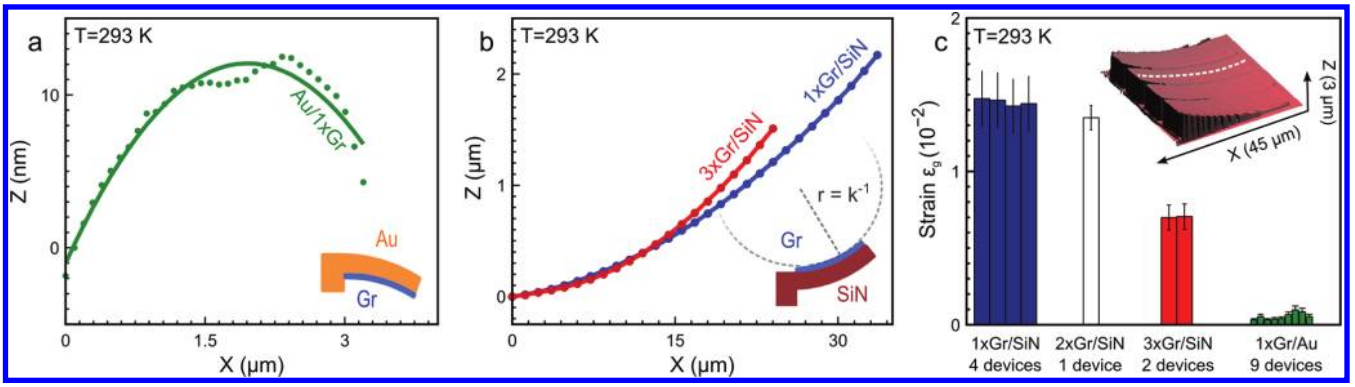

Figure 2. Probing the built-in strain of graphene deposited onto Au and SiN_x substrates. (a) Representative profile $Z(X)$ of a Au/1×Gr cantilever at room temperature immediately following fabrication, as obtained from interferometric profilometry. Dots are data points, solid line is a constant-curvature fit. Au cantilevers have a kink at the base that may be due to inelastic deformation during fabrication. (b) Same as (a) for 1×Gr/SiN_x and 3×Gr/SiN_x cantilevers. While the 1×Gr/SiN_x and the 3×Gr/SiN_x cantilevers are of the same length, differences in the sample tilt prevented us from collecting Z data at the end segment of the 3×Gr/SiN_x devices. (c) The strain in graphene on different substrates extracted from curvature via eq 1. Inset: A height map of 1×Gr/SiN_x cantilevers obtained via interferometric profilometry. The dashed line corresponds to the $Z(X)$ profile shown in (b).

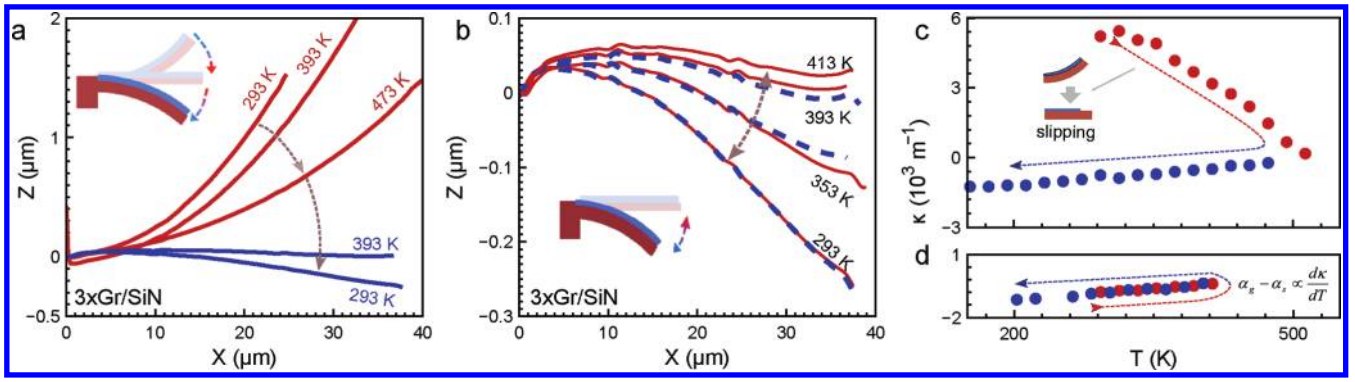

Figure 3. Temperature dependence of curvature for graphene bimetallic-like cantilevers. (a) Temperature dependence of the profile $Z(x)$ of a 3×Gr/SiN cantilever during the initial heating (red)/cooling (blue) cycle immediately after fabrication; the curvature κ extracted from the profile is shown in (c). Note the hysteretic behavior: κ at room temperature is reduced after heating and cooling. (b) The T-dependence of the profile for the same device in subsequent heating/cooling cycles; the corresponding curvature is shown in (d). The curvature data obtained during the heating cycle are artificially offset by 10 K to emphasize the nonhysteretic behavior of $\kappa(T)$.

To fabricate 1×Gr/SiN_x (2×Gr/SiN_x or 3×Gr/SiN_x) devices we successively transfer the target number of single layer graphene sheets grown by chemical vapor deposition (CVD) on copper foils[11] onto a suspended 188 nm thick, low-stress silicon nitride membrane supported by a silicon frame. Individual cantilevers are cut out of the membrane using a focused Ga ion beam. The fabrication procedure yields suspended cantilevers that are 5−8 μm wide and 30−40 μm long.

The fabrication procedure of 1×Gr/Au cantilevers starts by transferring a single layer of CVD-grown graphene onto a SiO_2(300 nm)/Si substrate. We pattern the graphene via a combination of electron-beam lithography and oxygen-plasma etching and then thermally evaporate a 50 nm thick layer of gold on top of the device. Cantilevers are released by etching 200 nm of the oxide in hydrofluoric acid.[12] The fabricated cantilevers are 2−3 μm wide and 2−4 μm long and are suspended 200 nm above the SiO_2 substrate.

In order to transfer graphene grown on copper foils onto either Au or SiN substrates we use an intermediary polymer (PMMA) support. A drop of PMMA in anisole solvent is deposited onto a copper foil and then heated to solidify the PMMA. Copper is then removed via chemical etching and the graphene/PMMA stack is placed onto a target substrate. Finally, PMMA is dissolved in acetone. It is important to note that the much larger thermal expansion coefficient of liquid compared to solid PMMA may generate a significant strain in graphene, even before it is deposited onto a target substrate (more fabrication details are provided in the Supporting Information).

We analyze the mechanical properties of graphene by examining the height profiles (Z) along the length direction (X) of the bimetallic-like cantilevers from 100 to 450 K in a nitrogen atmosphere. Interferometric profilometry (Wyko 9800, Veeco) is employed to obtain $Z(X)$ profiles with a vertical resolution of 0.1 nm (Figure 2c, inset). We observe three distinct trends in every device measured. First, immediately after fabrication and at room temperature T_0 = 293 K every cantilever is significantly bent (Figure 2). Second, after an initial annealing step the magnitude of bending is temperature-dependent (Figure 3). Third, in Gr/SiN_x cantilevers there are changes in the bending that are irreversible during the initial heating/cooling process but become reversible in successive temperature cycling (Figure 3c,d). We now quantitatively examine these trends and associate the first trend with the presence of significant built-in strain in graphene, the second with graphene's thermal expansion, and

dx.doi.org/10.1021/nl202562u |Nano Lett. XXXX, XXX, 000–000

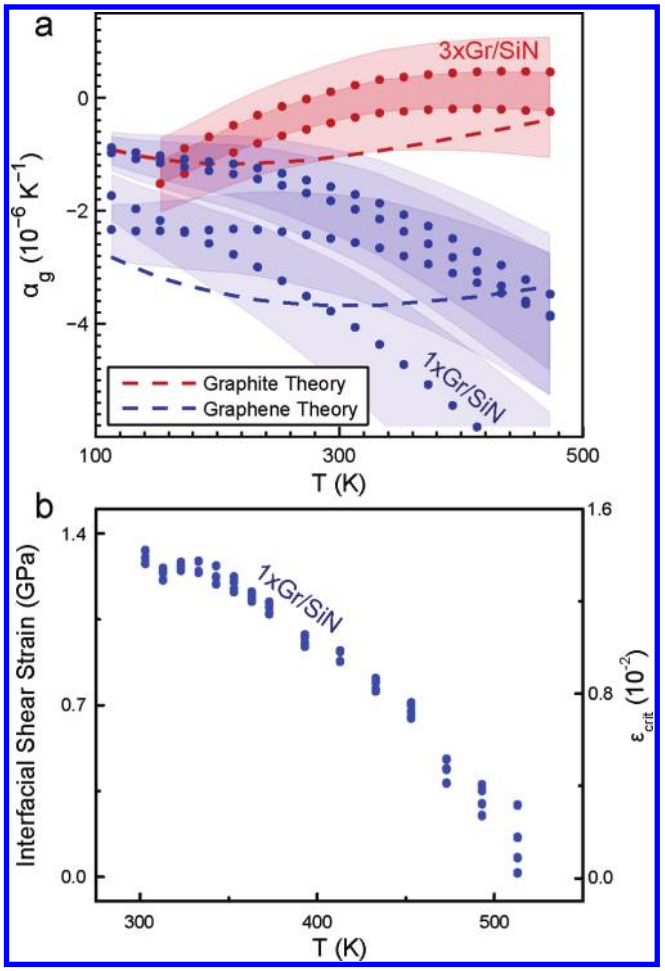

Figure 4. Extracting material parameters of graphene on substrates. (a) Linear thermal expansion coefficient α_g vs temperature T of single layer (blue circles) and three layer (red circles) graphene, as measured from multiple 1×Gr/SiN$_x$ and 3×Gr/SiN$_x$ devices. The shaded regions represent the uncertainty in α_g due to the uncertainty in the material parameters of our cantilevers, the blue and red dashed lines are theoretical expectations for α_g of graphene and graphite respectively.[18] (b) Interfacial shear strength and critical strain ε_{crit} that the 1×Gr/SiN interface supports as a function of temperature.

the third with slipping between graphene and the substrate at large strains.

We begin with the observation that immediately following fabrication every cantilever is not flat but is bent toward the graphene layer (Figures 2a,b). We associate this bending with the strain mismatch between graphene (ε_g) and the substrate (ε_s). A cantilever composed of unequally strained graphene and substrate layers is expected to minimize its energy by bending into an arc with a curvature κ (the inverse of radius of curvature, Figure 2b, inset) that is proportional to $\Delta\varepsilon = \varepsilon_g - \varepsilon_s$. The analytical solution is

$$\kappa = 6\frac{E_g t_g(1-\nu_s)}{E_s t_s^2(1-\nu_g)}\Delta\varepsilon \qquad (1)$$

where E_g, t_g, and ν_g (E_s, t_s, ν_s) are the Young's modulus, the thickness, and the Poisson ratio of the graphene (substrate) layer, respectively.[13] The observed profiles $Z(X)$ of all the cantilevers are indeed arcs with constant curvature κ (Figure 2a,b) and so the strain level of graphene ε_g can be determined as long as the material parameters of eq 1 are known.

Although eq 1 is derived for macroscopic materials, recent work on suspended graphene films suggests that such models are applicable to two-dimensional graphene assuming $E_g = 1 \pm 0.1$ TPa, $t_g = 0.35$ nm ($t_g = 1.05$ nm for three-layer graphene), and $\nu_g = 0.165$.[5,14] In a separate measurement, we determine the material parameters of our substrate materials to be $E_s = 220 \pm 13$ GPa, $t_s = 188 \pm 2$ nm, $\nu_s = 0.22$ for SiN$_x$ and $E_s = 25-45$ GPa, $t_s = 50 \pm 2$ nm, $\nu_s = 0.44$ for gold. We also measure the built in strain ε_s in as-deposited Au and SiN$_x$ to be small ($\varepsilon_s < 4 \times 10^{-4}$) compared to ε_g, such that $\Delta\varepsilon \sim \varepsilon_g$ (details provided in Supporting Information).

Using eq 1 to obtain ε_g from multiple data sets similar to Figure 2a,b, we find that the graphene layer in all measured cantilevers is under significant tensile strain that is significantly larger in 1×Gr/SiN$_x$ devices, $\varepsilon_g \sim 1.5 \times 10^{-2}$, compared to Au/1×Gr devices, $\varepsilon_g = 1 \times 10^{-3} - 4 \times 10^{-4}$ (Figure 2c). In the last part of the paper, we address this observation in detail and attribute it to a varying graphene-substrate interaction strength.

Next, we discuss a pronounced temperature dependence in the curvature of the cantilevers (Figure 3c,d) that is extracted from their $Z(X)$ profiles (Figure 3a,b). Initially, for the Gr/SiN$_x$ devices, this dependence is hysteretic; the curvature of the cantilevers at room temperature changes significantly when they are first heated to $T > 473$ K and does not return to its original value when cooled back to 293 K (Figure 3c). However, this hysteretic behavior disappears after the first heating and cooling cycle, and we observe that the cantilevers bend up and down reproducibly as they are heated and cooled multiple times between $T = 450$ K and 110 K without exhibiting any memory of their previous state (Figure 3b,d). The Gr/Au cantilevers behave nonhysteretically in the entire range of temperatures.

We first focus on the nonhysteretic temperature behavior (Figure 3d), which we ascribe to the mismatch of the coefficients of thermal expansion between graphene, $\alpha_g(T)$, and the substrate, $\alpha_s(T)$. As all materials tend to change their size with temperature as a result of thermal expansion, the strain difference between graphene and the substrate $\Delta\varepsilon$ is also temperature dependent

$$\Delta\varepsilon(T) = \int_{T_0}^{T}[\alpha_g(T) - \alpha_s(T)]\mathrm{d}T + \Delta\varepsilon_0 \qquad (2)$$

where $\Delta\varepsilon_0$ is the previously discussed difference in built-in strains between graphene and the substrate layers at room temperature. Thus, according to eq 1, we expect that the curvature κ of the cantilevers should indeed also be temperature dependent and that its temperature derivative $\mathrm{d}\kappa/\mathrm{d}T$ should be proportional to $\alpha_g(T) - \alpha_s(T)$. Assuming previously reported values for α_s,[15−17] we now extract the coefficient of thermal expansion of graphene using eqs 1 and 2.

Figure 4a shows $\alpha_g(T)$ of single layer and multilayer graphene on silicon nitride obtained from four 1×Gr/SiN$_x$ (blue curves) and two 3×Gr/SiN$_x$ (red curves) devices. The shaded regions represent uncertainty in α_g that result from uncertainties in the Young's modulus and thicknesses of our samples. We found α_g of single-layer graphene at room temperature to be negative (i.e., graphene shrinks when heated), in the range of $\alpha_g = (-5 \ldots -1) \times 10^{-6}$ K^{-1}, close to the theoretical expectation of $\alpha_g = -3.7 \times 10^{-6}$ K^{-1},[18] and smaller in magnitude than the previously reported data for suspended graphene devices.[6,7,19] For double- and triple-layer graphene we determine near-zero $|\alpha_g| < 7 \times 10^{-7}$ K^{-1}, close

dx.doi.org/10.1021/nl202562u |Nano Lett. XXXX, XXX, 000–000

to the value $\alpha_g = -1.2 \times 10^{-6}\,K^{-1}$ for the in plane coefficient of thermal expansion of bulk graphite.[18] From Au/1×Gr devices, we can only estimate the range of the thermal expansion coefficient of single layer graphene on gold, $-8 \times 10^{-6}\,K^{-1} < \alpha_g < 0$, due to the large uncertainty in the material parameters of gold.

Graphene's large negative coefficient of thermal expansion α_g is a consequence of the two-dimensional nature of graphene and is related to the contribution of the of the out-of-plane phonon modes (Lifshitz membrane effect).[18] In graphite these modes are quenched by the interlayer van der Waals interaction leading to a less negative α_g.[18] The affinity of the thermal expansion coefficients of graphene attached to the substrate to the theoretical expectation of α_g for a pristine suspended graphene membrane suggests that the coupling between graphene and the SiN_x substrate is relatively weak. Surprisingly, the small magnitudes of α_g that we observe in double- and triple- layer devices may indicate that the coupling between graphene layers and hence the suppression the out-of-plane modes in such devices is stronger than that in graphite.

We confirmed the validity of our mechanical model, eqs 1 and 2, and the accuracy of the tabulated values for substrate material parameters $E_s,\nu_s,\alpha_s(T)$ by fabricating and measuring multiple test devices. First, we fabricated suspended SiN_x cantilevers without the graphene layer on top and observed that these cantilevers are flat, as expected. Second, we examined some of the Au/1×Gr cantilevers where the graphene layer was removed by exposing the devices to ozone atmosphere. Such cantilevers also remained flat in the entire range of measurement temperatures. Third, we fabricated SiN_x/Au cantilevers and confirmed that their temperature-dependent curvature follows eqs 1 and 2. Finally, we performed finite element modeling of the cantilever geometry used in the experiments and confirmed that the computed height profile $Z(X)$ is within 3% of the profile predicted by eq 1 (details in the Supporting Information).

Having explored the nonhysteretic behavior of the graphene cantilevers, we now turn to the hysteretic temperature behavior (Figure 3a,c). Our key observation is that it occurs when the strain in graphene exceeds a critical strain ε_{crit}, which is temperature dependent.

Indeed, when $\varepsilon_g < \varepsilon_{crit}$ the cantilevers bend up and down according to eqs 1 and 2 as the devices are heated and cooled (Figure 3d, red and blue data points respectively). However, when $\varepsilon_g \geq \varepsilon_{crit}$, such as in the devices immediately following fabrication, the curvature of the cantilevers decreases when they are heated (Figure 3c, red points), contrary to the predictions of eqs 1 and 2, and does not return to the same value upon cooling (Figure 3c, blue data points).

We interpret the decrease in strain when $\varepsilon_g > \varepsilon_{crit}$ as graphene slipping along the substrate. When $\varepsilon_g > \varepsilon_{crit}$ the force due to strain exceeds the force acting on graphene due to the friction between graphene and the substrate. In that case, graphene delaminates from the substrate and relieves its strain by slipping. This is manifest by straightening of the cantilever or, equivalently, curvature decreasing with temperature $d\kappa/dT < 0$.

We measure the critical strain ε_{crit} as a function of T by heating and cooling the same devices multiple times to gradually increasing temperatures and determining the onset of the slipping behavior (right axis of Figure 4b; the original data in Supporting Information). We now use the measured values of ε_{crit} to roughly estimate the frictional forces between graphene and the substrate. To do so, we note that in order for graphene to slip, the local shear stress in graphene should become larger than the stress due to frictional forces, as quantified by the interfacial shear strength (IFSS) of the graphene/substrate interface. To obtain the numerical estimate of IFSS, we find the maximum shear stress in graphene in 1×Gr/SiN, 2×Gr/SiN, and 3×Gr/SiN devices using finite element analysis.

As expected, we find that the stress is concentrated at the end of the cantilever. Our data reveal a large IFSS of ∼1 GPa for the 1×Gr/SiN devices at room temperature (Figure 4b).[20,21] There is a clear weakening of the graphene/substrate friction with temperature that may be related to the weakening of chemical bonds attaching graphene to the substrate as we increased T. In light of IFSS we can understand the lower strain observed in the Au/Gr cantilevers as being related to a lower IFSS of the graphene/gold interface. Finally, the IFSS we estimate for graphene on silicon nitride is large and perhaps related to graphene's large adhesion energy.[23]

We note that while fabrication residues, such as remnants of PMMA resist, may be present on the surface of graphene devices,[24] we believe that these residues do not distort our measurement results. First, the processes of graphene transfer and fabrication leave the interface between graphene and the substrate uncontaminated allowing us to probe intrinsic graphene/substrate adhesion. Second, the Young's modulus of polymeric residues is negligible compared to the Young's modulus of either graphene or the substrate[7] and hence we do not expect distortion of strain of our devices due to the presence of these residues.

In conclusion, we note that the reported observations may have several interesting applications. First, the reported significant variation of strain in graphene deposited on different substrates may be exploited toward practical realization of the proposed strain-engineering scheme to control electron properties of graphene.[9] The observed variation in bending in composite graphene cantilevers as a function of temperature may be used to create novel types of NEMS switches and actuators. For example, graphene's minuscule thickness and large Young's modulus could enable very thin and therefore especially sensitive thermal and chemical sensors.[22,25,26] The temperature-induced bending of graphene/gold cantilevers may also explain the failure mechanism in large suspended graphene devices.[12] Finally, the ability to tune graphene's coefficient of thermal expansion by careful selection of the substrate material and number of graphene layers may be important in designing composite materials based on graphene.[3,4]

■ ASSOCIATED CONTENT

Supporting Information. Additional information and figures. This material is available free of charge via the Internet at http://pubs.acs.org.

■ AUTHOR INFORMATION

Corresponding Author
*E-mail: kirill.bolotin@vanderbilt.edu.

■ ACKNOWLEDGMENT

We thank Bin Wang, A.K.M. Newaz, and L.C. Feldman for enlightening discussions and Vanderbilt Institute of Nanoscale Science and Engineering for allowing use of their facilities. A portion of this research was conducted at the Center for

Nanophase Materials Sciences, which is sponsored at Oak Ridge National Laboratory by the Office of Basic Energy Sciences, U.S. Department of Energy. This research is supported in part by NSF DMR-1056859 and NSF EPS-1004083.

REFERENCES

(1) Novoselov, K.; et al. Two-dimensional gas of massless Dirac fermions in graphene. *Nature* **2005**, *438*, 197–200.
(2) Lee, C.; Wei, X.; Kysar, J. W.; Hone, J. Measurement of the elastic properties and intrinsic strength of monolayer graphene. *Science* **2008**, *321*, 385–388.
(3) Dikin, D.; et al. Preparation and characterization of graphene oxide paper. *Nature* **2007**, *448*, 457–460.
(4) Potts, J. R.; et al. Thermomechanical properties of chemically modified graphene/poly(methyl methacrylate) composites made by in situ polymerization. *Carbon* **2011**, *49*, 2615–2623.
(5) Bunch, J. S.; et al. Electromechanical resonators from graphene sheets. *Science* **2007**, *315*, 490–493.
(6) Singh, V.; et al. Probing thermal expansion of graphene and modal dispersion at low-temperature using graphene nanoelectromechanical systems resonators. *Nanotechnology* **2010**, *21*, 165204.
(7) Chen, C.; et al. Performance of monolayer graphene nanomechanical resonators with electrical readout. *Nat. Nanotechnol.* **2009**, *4*, 861–867.
(8) Jiang, J.-W.; Wang, J.-S.; Li, B. Young's modulus of graphene: A molecular dynamics study. *Phys. Rev. B* **2009**, *80*, 113405.
(9) Guinea, F.; Katsnelson, M.; Geim, A. Energy gaps and a zero-field quantum Hall effect in graphene by strain engineering. *Nat. Phys.* **2009**, *6*, 30–33.
(10) Levy, N.; et al. Strain-induced pseudo−magnetic fields greater than 300 T in graphene nanobubbles. *Science* **2010**, *329*, 544–547.
(11) Li, X.; et al. Large-area synthesis of high-quality and uniform graphene films on copper foils. *Science* **2009**, *324*, 1312–1314.
(12) Bolotin, K.; et al. Ultrahigh electron mobility in suspended graphene. *Solid State Commun.* **2008**, *146*, 351–355.
(13) Townsend, P. H.; Barnett, D. M.; Brunner, T. A. Elastic relationships in layered composite media with approximation for the case of thin films on a thick substrate. *J. Appl. Phys.* **1987**, *62*, 4438–4444.
(14) Blakslee, O.; Proctor, D.; Seldin, E.; Spence, G.; Weng, T. Elastic Constants of Compression-Annealed Pyrolytic Graphite. *J. Appl. Phys.* **2009**, *41*, 3373–3382.
(15) Martyniuk, M.; Antoszewski, J.; Musca, C. A.; Dell, J. M.; Faraone, L. Environmental stability and cryogenic thermal cycling of low-temperature plasma-deposited silicon nitride thin films. *J. Appl. Phys.* **2006**, *99*, 053519.
(16) Paszkowicz, W.; et al. Thermal expansion of spinel-type Si_3N_4. *Phys. Rev. B* **2004**, *69*, 052103.
(17) Nix, F. C.; MacNair, D. The thermal expansion of pure metals: Copper, gold, aluminum, nickel, and iron. *Phys. Rev.* **1941**, *60*, 597–605.
(18) Mounet, N.; Marzari, N. First-principles determination of the structural, vibrational and thermodynamic properties of diamond, graphite, and derivatives. *Phys. Rev. B* **2005**, *71*, 205214.
(19) Bao, W.; et al. Controlled ripple texturing of suspended graphene and ultrathin graphite membranes. *Nat. Nanotechnol.* **2009**, *4*, 562–566.
(20) Gong, L.; et al. Interfacial stress transfer in a graphene monolayer nanocomposite. *Adv. Mater.* **2010**, *22*, 2694–2697.
(21) Young, R. J.; et al. Strain mapping in a graphene monolayer nanocomposite. *ACS Nano* **2011**, *5*, 3079–3084.
(22) Lavrik, N. V.; Sepaniak, M. J.; Datskos, P. G. Cantilever transducers as a platform for chemical and biological sensors. *Rev. Sci. Instrum.* **2004**, *75*, 2229–2253.
(23) Koenig, S. P.; Boddeti, N. G.; Dunn, M. L.; Bunch, J. S. Ultrastrong Adhesion of Graphene Membranes. *Nature Nanotechnology*, **2011**, *6*(9), 543–546. Nature Publishing Group. doi: 10.1038/nnano.2011.123.
(24) Ishigami, M.; Chen, J. H.; Cullen, W. G.; Fuhrer, M. S.; Williams, E. D. Atomic structure of graphene on SiO_2. *Nano Lett.* **2007**, *7*, 1643–8.
(25) LeMieux, M. C.; et al. Polymeric nanolayers as actuators for ultrasensitive thermal bimorphs. *Nano Lett.* **2006**, *6*, 730–734.
(26) Singamaneni, S.; et al. Bimaterial microcantilevers as a hybrid sensing platform. *Adv. Mater.* **2008**, *20*, 653–680.